

# Glasma flux tubes and the near side ridge phenomenon at RHIC

Adrian Dumitru<sup>(1)</sup>, François Gelis<sup>(2)</sup>,  
Larry McLerran<sup>(3,4)</sup>, Raju Venugopalan<sup>(3)</sup>

April 24, 2008

1. Institut für Theoretische Physik, J. W. Goethe Universität  
Max-von Laue-Str. 1, D-60438, Frankfurt am Main, Germany
2. Theory Division, PH-TH, Case C01600, CERN  
CH-1211, Geneva 23, Switzerland
3. Physics Department, Building 510A  
Brookhaven National Laboratory, Upton, NY-11973, USA
4. RIKEN Brookhaven Research Center, Building 510A  
Brookhaven National Laboratory, Upton, NY 11973, USA

## Abstract

We investigate the consequences of long range rapidity correlations in the Glasma. Particles produced locally in the transverse plane are correlated by approximately boost invariant flux tubes of longitudinal color electric and magnetic fields that are formed when two sheets of Colored Glass Condensate pass through one another, each acquiring a modified color charge density in the collision. We argue that such long range rapidity correlations persist during the evolution of the Quark Gluon Plasma formed later in the collision. When combined with transverse flow, these correlations reproduce many of the features of the recently observed ridge events in heavy ion collisions at RHIC.

Preprint CERN-PH-TH-2008-083.

## 1 Introduction

Among the more striking features in cosmology are the large scale fluctuations seen in the cosmological microwave background (CMB) and in the mass density perturbations that result in galaxies. Such large scale fluctuations are at first sight hard to understand because they extend over much larger distance scales than could be set up by interactions of the thermal medium produced

after the big bang. It is now believed that these large scale fluctuations originate in small quantum fluctuations present during the inflationary epoch. During the rapid expansion of the universe in this epoch, these quantum fluctuations were stretched to size scales much larger than those that were causally connected in the post-inflationary era when the universe was expanding in a state close to thermal equilibrium. Therefore such super horizon scale fluctuations cannot be much affected by the sub-horizon scale processes allowable in the post-inflationary thermal universe. This explains why CMB measurements provide extremely valuable information about the inflationary epoch of the universe, despite the fact that the CMB radiation was produced long after ( $t_{\text{CMB}} \sim 4 \cdot 10^5$  years) the primordial fluctuations that are responsible for its features ( $t_{\text{inflation}} \sim 10^{-33}$  seconds).

There is a concrete analog of such super-horizon fluctuations in the matter produced in high energy hadronic collisions such as heavy ion collisions at RHIC, as illustrated in fig. 1. In this figure, we represent the “event horizons” as seen

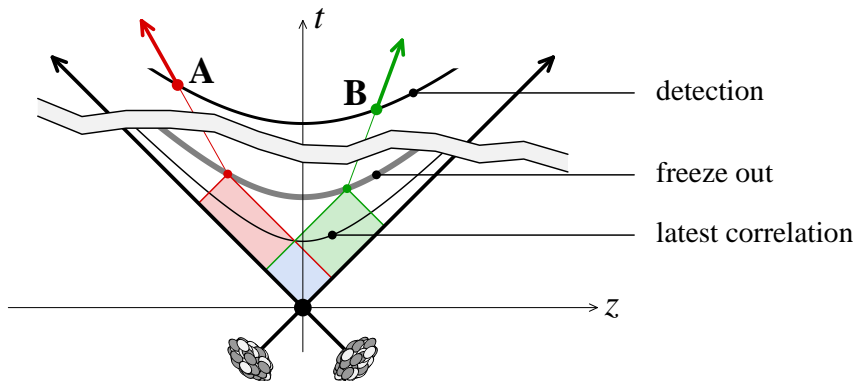


Figure 1: The red and green cones are the location of the events in causal relationship with the particles  $A$  and  $B$  respectively. Their intersection is the location in space-time of the events that may correlate the particles  $A$  and  $B$ .

from the last rescattering of two particles  $A$  and  $B$  on the freeze-out surface. These are the red and green cones pointing to the past. Any event that has a causal influence on the particles  $A$  or  $B$  must take place inside the corresponding event horizon. Any event that induces a correlation between the particles  $A$  and  $B$  must lie in the overlap of their event horizons. Therefore, if the particles  $A$  and  $B$  have rapidities  $y_A$  and  $y_B$ , the processes that caused their correlations must have occurred before the time<sup>1</sup>

$$\tau \leq \tau_{\text{freeze out}} e^{-\frac{1}{2}|y_A - y_B|}. \quad (1)$$

<sup>1</sup>We assume here that a particle detected with momentum rapidity  $y$  originates from a point of space-time rapidity  $\eta \approx y$  on the freeze-out surface. This is a consequence of the boost invariance of the collision (at high energy), and of the fact that the local thermal motion spreads the rapidities by at most one unit in rapidity.

Therefore, we see that long range rapidity correlations can only be created at early times—shortly after the collision or even in the wavefunctions of the incoming projectiles, that form sheets of Color Glass Condensate [1]-[3] at high energies. In a high energy collision of these Color Glass Condensates, an interacting and evolving system of high intensity color electric and color magnetic fields is produced [4]-[12]. This collection of primordial fields is the Glasma [8,9], and initially it is composed of only rapidity independent longitudinal color electric and magnetic fields. These fields generate topological Chern-Simons charge [13]. Correlations associated with particle production from these fields span large distances in rapidity. In contrast, due to the longitudinal expansion of the matter produced in RHIC collisions, thermal effects can only affect particle correlations on a distance scale of approximately one unit of rapidity.

Because the longitudinal fields are approximately rapidity invariant, there are long range correlations built into the initial conditions—these inevitably have their origin in the quantum mechanical wavefunctions of the hadrons. Of course, the long range correlations are only approximately rapidity invariant. A proper treatment of quantum fluctuations in the hadron wavefunctions suggests that the characteristic distance scales—beyond which one has significant variations in the correlation—is of order  $1/\alpha_s(Q_s)$ . Here  $Q_s$  is the saturation momentum of partons in the nuclear wavefunctions; it grows rapidly with both the energy and the nuclear size. The strong interaction strength  $\alpha_s(Q_s)$  is therefore correspondingly weak for nuclear collisions or very high energy hadron-hadron collisions resulting in a characteristic distance scale of several units in rapidity for the rapidity correlations.

The existence of long range rapidity correlations in high energy hadronic collisions has been measured in ISR experiments [15], and is intrinsic to string models of high energy collisions such as the Lund model and the Dual Parton Model [16]-[17]. The essential new feature of the Glasma is that the fields are localized in the transverse scale over distances (of order  $1/Q_s$ ) that are smaller than the nucleon size. Because the dynamics of these fields in collisions at high energies or for large nuclei occurs at small transverse distances, this dynamics can be described by a weak coupling expansion. A further point of departure is that in addition to the longitudinal color electric fields envisioned in the Dual Parton model and the Lund model, there is a longitudinal magnetic field of equal intensity. It is this combination of electric and magnetic fields that generates a finite topological charge density.

Such topologically distinct field configurations are of great interest in several areas of theoretical physics. For example, the analog of these fields in electroweak theory may be responsible for generating the baryon asymmetry of the universe [18]-[19]. In QCD, they may be the source of masses of hadrons [20].

Recent experimental studies have shown that there are long range rapidity correlations at RHIC [21]. In the STAR experiment, forward-backward correlations in the total multiplicity were studied as a function of centrality in Au-Au collisions. A strong correlation was found, which increases significantly with greater collision centrality. This correlation is stronger than expected from Monte-Carlo models of particle production. This effect can be understood as

arising from the interference between the classical contribution of rapidity independent Glasma fields, and the first order quantum correction to this result. The latter is short ranged in rapidity [22].

More specifically, the forward backward correlation as a function of the rapidities at which the multiplicity is measured is

$$C_{\text{FB}}(y_1, y_2) = \frac{\left\langle \frac{dN}{dy_1} \frac{dN}{dy_2} \right\rangle}{\left\langle \frac{dN}{dy_1} \frac{dN}{dy_2} \right\rangle_{y'_1=y'_2=y}}, \quad (2)$$

where  $dN/dy_1$  and  $dN/dy_2$  are measured in a single event,  $y$  is typically chosen to be the midpoint between  $y_1$  and  $y_2$  and the brackets denote the average over events. The denominator normalizes the expression such that  $C(y, y) = 1$ . If classical fields dominated this correlation function, then  $C(y_1, y_2) = 1$  since the initial Glasma fields are boost invariant. However, as mentioned, there is a short range contribution to  $C_{\text{FB}}(y_1, y_2)$  arising from quantum corrections which is of order  $\alpha$ . Thus  $C_{\text{FB}}(y_1, y_2)$  is typically less than unity because for long range rapidity correlations the numerator of this expression only contains the long range contribution while the denominator, corresponding to zero separation in rapidity, is a sum of both short range and long range contributions. For events in nuclear collisions with increasing centrality, the coupling constant gets progressively smaller, thereby leading to a diminished contribution of the short range correlation relative to the long range classical correlation. Thus  $C_{\text{FB}}(y_1, y_2)$  approaches unity with increasing centrality of the collision. Such a forward-backward correlations, while consistent with the Glasma hypothesis, is perhaps not as direct a verification of the longitudinal electric and magnetic fields as might be desired. We will argue in this paper that so called “ridge” events discovered by STAR may provide a more direct confirmation of this fundamental property of the Glasma.

These striking “ridge” events were revealed in studies of the near side spectrum of correlated pairs of hadrons by the STAR collaboration [23,24]. The spectrum of correlated pairs on the near side of the detector (defined by an accompanying unquenched jet spectrum) extends across the entire detector acceptance in pseudo-rapidity of order  $\Delta\eta \sim 2$  units but is strongly collimated for azimuthal angles  $\Delta\phi$ . Preliminary analyses of measurements by the PHENIX [25] and PHOBOS [26] collaborations appear to corroborate the STAR results. In the latter case, with a high momentum trigger, the ridge is observed to span the even wider PHOBOS acceptance in pseudo-rapidity of  $\Delta\eta \sim 6$  units.

A plot of the ridge in the  $\eta - \phi$  plane is shown in fig. 2(a). The quantity  $\Delta\rho/\sqrt{\rho_{ref}}$  plotted as a function of rapidity and azimuthal angle, is the density of particles correlated with a particle emitted at zero rapidity [43]. All particles with  $p_{\perp} \geq 150$  MeV are included. The quantity  $\Delta\rho$  is the difference in densities between single events and mixed events. The quantity  $\rho_{ref}$  comes from mixed events. The results are corrected for the effects of azimuthally asymmetric flow. As shown in fig. 2(b), an important feature of the ridge is that its height is strongly dependent on centrality. As the centrality of the heavy ion collision

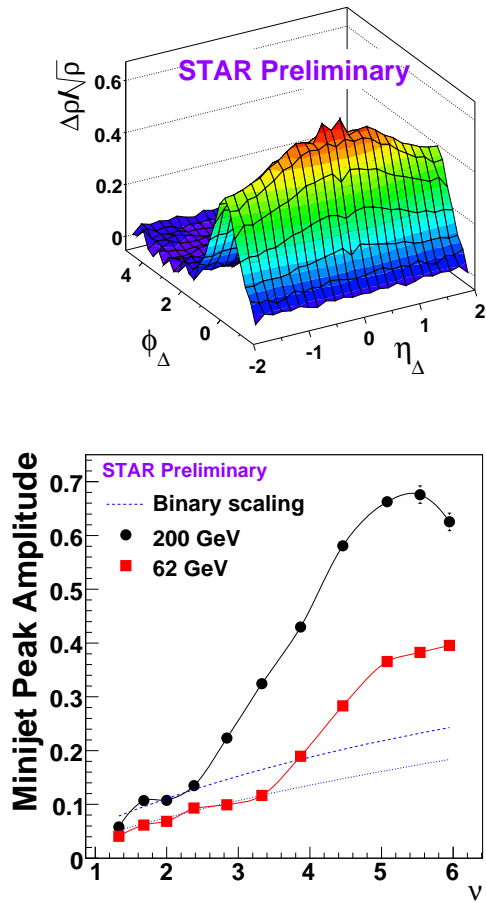


Figure 2: (a) Top Figure: The ridge as seen in the measurement of two particle correlations with minimal cut on particle momenta. Mixed events have been subtracted, as have been the effects of azimuthally asymmetric flow. The centrality bin here is 19-28% b) Bottom Figure: The height of the ridge as a function of the number of binary collisions per participant. Both figures are preliminary STAR figures from Ref. [43]

is increased, there is a rapid transition to the regime of long range rapidity correlations; there is an equally distinct, if less dramatic, collimation of the width in  $\Delta\phi$  with increasing centrality, as shown in fig. 3.

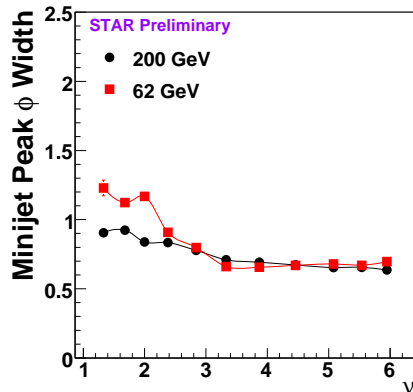


Figure 3: The width in rapidity and azimuthal angle of the ridge as a function of the number of binary collisions per participant.

These features of the ridge are not seen in proton–proton or deuteron–gold collisions and appear to be unique to nucleus–nucleus collisions. As mentioned previously, long range rapidity correlations are not unique to nucleus–nucleus collisions and have been seen in proton–proton collisions as far back as the Intersecting Storage Ring (ISR) experiments at CERN [15]. However, in that case, the correlations are not collimated in azimuthal angle and therefore do not have the striking ridge like structure observed at RHIC.

In this paper, we argue that the ridge is formed as a consequence of both long range rapidity correlations that are generic in hadronic and nuclear collisions at high energies plus the radial flow of the hot partonic matter that is specific to high energy nuclear collisions. Here we deal exclusively with the ridge as seen in the total multiplicity of associated particles (with a minimum  $p_{\perp}$  cutoff as low as 150 MeV). This has the advantage for us that the multiplicity density of particles associated with the ridge should be approximately conserved. A discussion of the ridge for high transverse momentum particles, while possible in our formalism, is complicated due to the interaction of such high momenta particles with the media, where there is energy loss.

In our simple picture, the longitudinal electric and magnetic fields of the Glasma form flux tubes that emit a radiation spectrum isotropic in the relative azimuthal angle between the particle pairs. While of finite amplitude, such a distribution would appear featureless on a plot of the spectrum in the  $\Delta\eta$ - $\Delta\phi$  plane. The collimation in  $\Delta\phi$  is a consequence of strong final state effects in the medium produced in nuclear collisions. For the particular effect we describe,

we will see that it is a consequence of strong radial flow in the medium as also previously suggested in the literature [27,29,28]. Besides the strong medium effect on the  $\Delta\phi$  distribution, increasing the centrality of nuclear collisions also enhances long range rapidity correlations; these are proportional to  $1/\alpha_s^2(Q_s^2)$ . Because the saturation scale is  $Q_s^2 \propto L$ , where  $L$  is thickness of the projectiles along the beam axis at a given impact parameter<sup>2</sup>, the average  $Q_s^2$  grows with increasing centrality, leading to stronger long range rapidity correlations.

Our computation of the correlated two particle distribution function for  $p_\perp, q_\perp \geq Q_s$  gives a result of the form<sup>3</sup>

$$\begin{aligned} & \left\langle \frac{dN_2}{dy_p d^2\mathbf{p}_\perp dy_q d^2\mathbf{q}_\perp} \right\rangle - \left\langle \frac{dN}{dy_p d^2\mathbf{p}_\perp} \right\rangle \left\langle \frac{dN}{dy_q d^2\mathbf{q}_\perp} \right\rangle \\ &= \kappa \frac{1}{S_\perp Q_s^2} \left\langle \frac{dN}{dy_p d^2\mathbf{p}_\perp} \right\rangle \left\langle \frac{dN}{dy_q d^2\mathbf{q}_\perp} \right\rangle. \end{aligned} \quad (3)$$

The quantity  $\kappa$  is a constant which we shall compute explicitly. The factor of  $1/S_\perp Q_s^2$  has the simple physical interpretation of the area of the flux tube from which the particles are emitted divided by the overall area of the system<sup>4</sup>. The Glasma flux tubes are illustrated in fig. 4.

The quantity  $\frac{\Delta\rho}{\sqrt{\rho_{ref}}}$  is equivalent to the left hand side of eq. (3) divided by  $\left\langle \frac{dN}{dy_p d^2\mathbf{p}_\perp} \right\rangle \left\langle \frac{dN}{dy_q d^2\mathbf{q}_\perp} \right\rangle$ , and multiplied by the multiplicity per unit rapidity,

$$\left\langle \frac{dN}{dy} \right\rangle = \frac{\kappa'}{\alpha_s(Q_s)} S_\perp Q_s^2, \quad (4)$$

where  $\kappa' \approx 1/13.5$  for an  $SU(3)$  gauge theory [45]. We therefore obtain

$$\frac{\Delta\rho}{\sqrt{\rho_{ref}}} = \frac{K_N}{\alpha_s} \quad (5)$$

where we shall show that  $K_N$  is a constant of order unity.

This relationship is basically a consequence of dimensionality—the correlations are due to a classical effect and there is only one dimensional scale which characterizes the Glasma. This formula is not corrected for transverse flow, which modifies this result, as we shall demonstrate, by introducing a dependence of the result on the azimuthal angle between the pairs.

As mentioned, our mechanism for the ridge has features in common with the work of Voloshin [27] and Shuryak [28]. However, as we shall discuss, there are important qualitative and quantitative differences with this approach. We also

<sup>2</sup>See Ref. [32] and references therein.

<sup>3</sup>Our definition of the differential two particle correlation is such that

$$\int d^2\mathbf{p}_\perp dy_p d^2\mathbf{q}_\perp dy_q \frac{dN_2}{dy_p d^2\mathbf{p}_\perp dy_q d^2\mathbf{q}_\perp} = N^2.$$

<sup>4</sup>Note that the right hand side is proportional to the area since the total multiplicity per unit rapidity scales as the area.

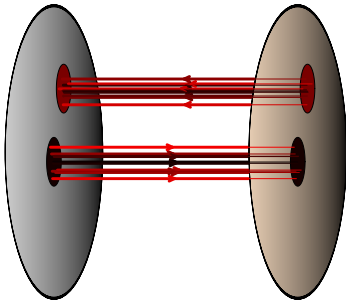


Figure 4: Glasma flux tubes. The transverse size of the flux tubes is of order  $1/Q_s$ .

note that there are several other models of the ridge [30]-we will not attempt to discuss these here. A key difference between the dominant particle production mechanism we will describe here and other mechanisms described in the literature is that our correlation is not formed from a daughter particle splitting off a parent particle. Instead, the dominant QCD contribution to the long range rapidity correlation comes from particles that are produced independently along the length of flux tube of color electric and magnetic fields, localized in a region of size  $1/Q_s$  in the transverse plane of the colliding nuclei.

## 2 Computing the Glasma 2-particle correlation

We now turn to a quantitative analysis of two particle correlations in the Glasma and their role in forming the near side ridge in A–A collisions. The variance of the two particle multiplicity distribution, for two particles with momenta  $\mathbf{p}$  and  $\mathbf{q}$ , is defined as

$$C(\mathbf{p}, \mathbf{q}) \equiv \left\langle \frac{dN_2}{dy_p d^2\mathbf{p}_\perp dy_q d^2\mathbf{q}_\perp} \right\rangle - \left\langle \frac{dN}{dy_p d^2\mathbf{p}_\perp} \right\rangle \left\langle \frac{dN}{dy_q d^2\mathbf{q}_\perp} \right\rangle, \quad (6)$$

where the brackets  $\langle \dots \rangle$  denote an average over events. Also, see footnote 3.

The contributions to  $C(\mathbf{p}, \mathbf{q})$  have distinct origins. If we compute emission in a fixed configuration of the color sources, there are connected and disconnected pieces. These are shown in fig. 5. The top diagram is disconnected and we might naively think it would contribute only to the uncorrelated second term of the above equation. This is not true because, when we average over the color sources, there are contributions which involve contractions of the sources between the two superficially disconnected diagrams. It is these contractions which dominate the computation of  $C(\mathbf{p}, \mathbf{q})$  because they arise from a classical contribution and are therefore leading order in powers of  $\alpha_s$ . The bottom diagram involves an interference between a connected and a disconnected diagram



and is suppressed by a power of the coupling<sup>5</sup>. In fact, a more sophisticated renormalization group treatment [34] shows that by computing only the classical contribution (top diagram of fig. 5) to  $C(\mathbf{p}, \mathbf{q})$ , and by averaging it with evolved distributions of sources with rapidity, one is automatically including both the leading logarithmic terms of the bottom diagram as well as the leading logs from NLO correction to the top diagram. Therefore, in the rest of this paper, we consider only the top diagram of fig. 5.

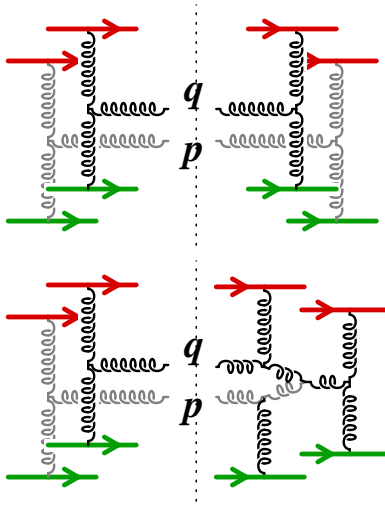


Figure 5: Top Figure: A classical diagram which yields a non-vanishing two particle correlation after averaging over the color sources. Bottom Figure: A contribution to the correlation function associated with a quantum correction to the classical field.

The classical contribution in  $C(\mathbf{p}, \mathbf{q})$  can be computed analytically<sup>6</sup> for  $Q_s \ll p_\perp, q_\perp$ . For  $p_\perp, q_\perp \leq Q_s$ , the computation is non-perturbative and must be performed numerically. Techniques developed previously [5–7] to compute single inclusive gluon can be extended to this case. Nevertheless, it is instructive to compute  $C(\mathbf{p}, \mathbf{q})$  in the large momentum region for several reasons. It will demonstrate that the effect is genuine, and we believe key features will persist at lower pair momenta even if numerical coefficients may be different in the two regimes. Also, as the ridge likely persists for high momentum hadron pairs [35], our computation may have direct application to that case modulo the energy loss effects mentioned previously.

<sup>5</sup>In the figure shown, we have kept only those diagrams which do not vanish under pairwise contraction of sources. There may be additional terms which involve contraction of three sources, but these are suppressed in simple models of the source color charge distribution and we do not therefore include them here.

<sup>6</sup>It can also be computed analytically for either  $p_\perp$  or  $q_\perp \gg Q_s$  but we shall not discuss that case here.

The correlated two particle inclusive distribution can be expressed as

$$C(\mathbf{p}, \mathbf{q}) = \frac{1}{4(2\pi)^6} \sum_{a, a'; \lambda, \lambda'} \left( \langle |\mathcal{M}_{\lambda\lambda'}^{aa'}(\mathbf{p}, \mathbf{q})|^2 \rangle - \langle |\mathcal{M}_\lambda^a(\mathbf{p})|^2 \rangle \langle |\mathcal{M}_{\lambda'}^{a'}(\mathbf{q})|^2 \rangle \right), \quad (7)$$

where the classical contribution to the amplitude for the production of a pair of gluons with momenta  $\mathbf{p}$  and  $\mathbf{q}$  is

$$\begin{aligned} \mathcal{M}_{\lambda\lambda'}^{aa'}(\mathbf{p}, \mathbf{q}) &= \epsilon_\mu^\lambda(\mathbf{p}) \epsilon_\nu^{\lambda'}(\mathbf{q}) p^2 q^2 A^{\mu, a}(\mathbf{p}) A^{\nu, a'}(\mathbf{q}), \\ \mathcal{M}_\lambda^a(\mathbf{p}) &= \epsilon_\mu^\lambda(\mathbf{p}) p^2 A^{\mu, a}(\mathbf{p}). \end{aligned} \quad (8)$$

Here the  $\epsilon$ 's are the polarization vectors of the gluons and  $a, a'$  are the color indices of the gauge fields. The average  $\langle \dots \rangle$  in eq. (7) is an average over the color configurations of the two nuclei; this average will be discussed further shortly.

At large transverse momenta, the classical gauge fields produced in the nuclear collision can be expressed explicitly [4,36,37] as

$$p^2 A^{\mu, a}(\mathbf{p}) = -i f_{abc} \frac{g^3}{2} \int \frac{d^2 \mathbf{k}_\perp}{(2\pi)^2} L^\mu(\mathbf{p}, \mathbf{k}_\perp) \frac{\tilde{\rho}_1^b(\mathbf{k}_\perp) \tilde{\rho}_2^c(\mathbf{p}_\perp - \mathbf{k}_\perp)}{\mathbf{k}_\perp^2 (\mathbf{p}_\perp - \mathbf{k}_\perp)^2}. \quad (9)$$

Here  $f_{abc}$  are the SU(3) structure constants,  $L^\mu$  is the well known<sup>7</sup> Lipatov vertex [38] and  $\tilde{\rho}_1, \tilde{\rho}_2$  are respectively the Fourier transforms of the color charge densities in the two nuclei [3]. Taking the modulus squared of eq. (8), summing over the polarizations and color indices, the first term in eq. (7) can be expressed as

$$\begin{aligned} C(\mathbf{p}, \mathbf{q}) &= \frac{g^{12}}{64(2\pi)^6} (f_{abc} f_{a'\bar{b}\bar{c}} f_{a\bar{b}\bar{c}} f_{a'\bar{b}\bar{c}}) \int \prod_{i=1}^4 \frac{d^2 \mathbf{k}_{i\perp}}{(2\pi)^2 \mathbf{k}_{i\perp}^2} \\ &\times \frac{L_\mu(\mathbf{p}, \mathbf{k}_{1\perp}) L^\mu(\mathbf{p}, \mathbf{k}_{2\perp})}{(\mathbf{p}_\perp - \mathbf{k}_{1\perp})^2 (\mathbf{p}_\perp - \mathbf{k}_{2\perp})^2} \\ &\times \frac{L_\nu(\mathbf{q}, \mathbf{k}_{3\perp}) L^\nu(\mathbf{q}, \mathbf{k}_{4\perp})}{(\mathbf{q}_\perp - \mathbf{k}_{3\perp})^2 (\mathbf{q}_\perp - \mathbf{k}_{4\perp})^2} \mathcal{F}_{b\bar{b}\bar{b}\bar{b}}^{c\bar{c}\bar{c}\bar{c}}(\mathbf{p}, \mathbf{q}; \{\mathbf{k}_{i\perp}\}). \end{aligned} \quad (10)$$

The scalar product of two Lipatov vectors is

$$L_\mu(\mathbf{p}, \mathbf{k}_\perp) L^\mu(\mathbf{p}, \mathbf{l}_\perp) = -\frac{4}{\mathbf{p}_\perp^2} [\delta^{ij} \delta^{lm} + \epsilon^{ij} \epsilon^{lm}] \mathbf{k}_\perp^i (\mathbf{p}_\perp - \mathbf{k}_\perp)^j \mathbf{l}_\perp^l (\mathbf{p}_\perp - \mathbf{l}_\perp)^m, \quad (11)$$

and we denote

$$\begin{aligned} \mathcal{F}_{b\bar{b}\bar{b}\bar{b}}^{c\bar{c}\bar{c}\bar{c}}(\mathbf{p}, \mathbf{q}; \{\mathbf{k}_{i\perp}\}) &\equiv \left\langle \tilde{\rho}_1^{*\hat{b}}(\mathbf{k}_{2\perp}) \tilde{\rho}_1^{*\bar{b}}(\mathbf{k}_{4\perp}) \tilde{\rho}_1^b(\mathbf{k}_{1\perp}) \tilde{\rho}_1^{\bar{b}}(\mathbf{k}_{3\perp}) \right. \\ &\times \left. \tilde{\rho}_2^{*\hat{c}}(\mathbf{p}_\perp - \mathbf{k}_{2\perp}) \tilde{\rho}_2^{*\bar{c}}(\mathbf{q}_\perp - \mathbf{k}_{4\perp}) \tilde{\rho}_2^c(\mathbf{p}_\perp - \mathbf{k}_{1\perp}) \tilde{\rho}_2^{\bar{c}}(\mathbf{q}_\perp - \mathbf{k}_{3\perp}) \right\rangle. \end{aligned} \quad (12)$$

---

<sup>7</sup>The components of this four vector are given explicitly by  $L^+(\mathbf{p}, \mathbf{k}_\perp) = -\frac{\mathbf{k}_\perp^2}{p^+}$ ,  $L^-(\mathbf{p}, \mathbf{k}_\perp) = \frac{(\mathbf{p}_\perp - \mathbf{k}_\perp)^2 - \mathbf{p}_\perp^2}{p^+}$ ,  $L^i(\mathbf{p}, \mathbf{k}_\perp) = -2 \mathbf{k}_\perp^i$ .

The average in eq. (12) corresponds to

$$\langle \mathcal{O} \rangle \equiv \int [D\rho_1 D\rho_2] W[\rho_1] W[\rho_2] \mathcal{O}[\rho_1, \rho_2]. \quad (13)$$

In the MV model [1,2],

$$W[\rho] \equiv \exp\left(-\int d^2\mathbf{x}_\perp \frac{\rho^a(\mathbf{x}_\perp)\rho^a(\mathbf{x}_\perp)}{2\mu_A^2}\right), \quad (14)$$

where  $\rho$  can be either  $\rho_1$  or  $\rho_2$ . The color charge squared per unit area  $\mu_A^2$ , besides the nuclear radius  $R$ , is the only dimensionful scale in the problem—as we will discuss later, the saturation scale  $Q_s$  can be expressed simply in terms of this scale. We will consider this Gaussian model in the rest of this paper<sup>8</sup>. For these Gaussian correlations, in momentum space,

$$\langle \tilde{\rho}^{*a}(\mathbf{k}_\perp) \tilde{\rho}^b(\mathbf{k}'_\perp) \rangle = (2\pi)^2 \mu_A^2 \delta^{ab} \delta(\mathbf{k}_\perp - \mathbf{k}'_\perp). \quad (15)$$

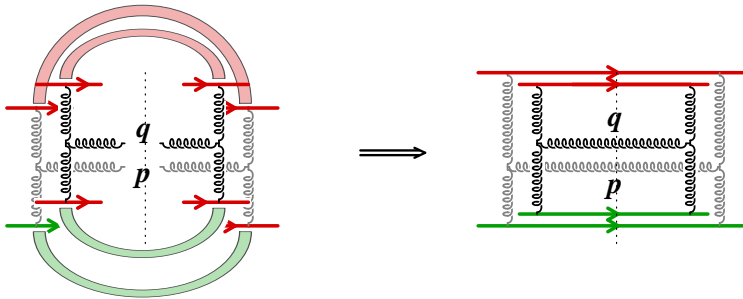


Figure 6: Trivial color correlation. This type of connection between the sources leads to a non correlated contribution to the 2-gluon spectrum, that cancels in the difference in eq. (6).

Examining the structure of  $\mathcal{F}$  in eq. (12), one observes that one of the nine possible quadratic combinations of the  $\rho_1$ 's and  $\rho_2$ 's is a disconnected piece, represented in the fig. 6, whose expression is nothing but

$$\langle |A(\mathbf{p})|^2 \rangle \langle |A(\mathbf{q})|^2 \rangle, \quad (16)$$

which is identical to the product of single inclusive distributions. It exactly cancels the disconnected contribution to pair production—the second term in eq. (7). Therefore only eight terms contribute to the correlated distributions of pairs. Of these, as we shall see, four terms give identical leading contributions to  $C_1(\mathbf{p}, \mathbf{q})$  for large  $p, q \gg Q_s$ . Two of these terms, as shown in fig. 7(a), have a

<sup>8</sup>In the simplest treatment of small  $x$  evolution, based on the Balitsky-Kovchegov equation [39],  $W[\rho]$  can also be modelled by a Gaussian [37], albeit non-local, with  $\mu_A^2 \rightarrow \mu_A^2(x_\perp)$ .

topology corresponding to diffractive scattering off quarks localized in a region  $1/Q_s$  in the nuclei. There is a rapidity gap between the produced particles and the scattered quarks in one of the nuclei or the other. The quarks on opposite sides of the cut may be localized at different transverse positions<sup>9</sup>. The other two terms with leading contributions have the structure of an interference graph depicted in fig. 7(b).

Of the four remaining terms, two are suppressed respectively by additional powers of  $p$  and  $q$  and two give  $\delta$ -function contributions for  $\vec{p} = \pm\vec{q}$ . The delta function terms are also suppressed relative to the terms we keep at large  $p$  and  $q$ , and would give a contribution not localized in the transverse coordinate, so that they would give a flat background once flow effects were included. Both of these types of contributions are represented in fig. 8 and are computed in Appendix B. We also address there subtleties related to the possible singular nature of these contributions.

The four leading contributions are computed in Appendix A and are shown to be identical. So, multiplying eq. 31 by a factor of four, we obtain the leading two particle Glasma correlation to be

$$C(\mathbf{p}, \mathbf{q}) = \frac{S_\perp}{(2\pi)^6} \frac{(g^2\mu_A)^8}{g^4 Q_s^2} \frac{\pi N_c^2(N_c^2 - 1)}{p_\perp^4 q_\perp^4}. \quad (17)$$

The relation of  $g^2\mu_A$  to  $Q_s$  can be quantified numerically by computing Wilson line correlators in the nuclear wavefunction. A careful comparison [45] (see also Ref. [46]) gives  $Q_s \approx 0.57 g^2\mu_A$ . It is instructive to express the result in eq. (17) in terms of the inclusive single gluon spectrum. This is the Gunion-Bertsch [41] result and has been computed previously in the CGC framework [4,11,42] to have the form

$$\left\langle \frac{dN}{dy_p d^2\mathbf{p}_\perp} \right\rangle = \frac{S_\perp}{8\pi^4} \frac{(g^2\mu_A)^4}{g^2} \frac{N_c(N_c^2 - 1)}{p_\perp^4} \ln \left( \frac{p_\perp}{Q_s} \right). \quad (18)$$

Substituting eqs. (6), (17) and (18) in eq. (3),

$$C(\mathbf{p}, \mathbf{q}) = \frac{\kappa}{S_\perp Q_s^2} \left\langle \frac{dN}{dy_p d^2\mathbf{p}_\perp} \right\rangle \left\langle \frac{dN}{dy_q d^2\mathbf{q}_\perp} \right\rangle, \quad (19)$$

we find  $\kappa \sim 4$ . Identifying the theoretical error on this number is difficult at this stage; it requires a numerical computation two particle correlations by solving classical Yang-Mills equations as was previously performed for single inclusive gluon production [5–7].

As we discussed previously, what is measured experimentally is the ratio of correlated pairs to the square root of the product of mixed pairs, defined as  $\Delta\rho/\sqrt{\rho_{\text{ref}}}$ , where  $\Delta\rho$  is the difference between the density of measured pairs minus mixed pairs and  $\rho_{\text{ref}}$  denotes the product of the density of mixed pairs [43].

---

<sup>9</sup>This only makes sense [40] within the framework of an effective theory where one is not sensitive to diffractive excitations over some typical transverse scale of size  $1/Q_s$ .

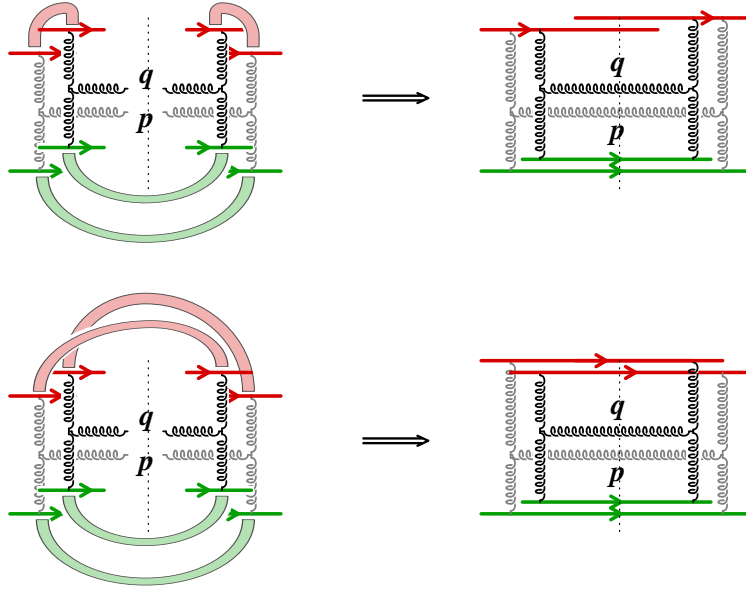


Figure 7: Topology of color correlations. These contributions are detailed in Appendix A. The upper (lower) contractions are pairwise contractions of  $\rho_1$  ( $\rho_2$ ). a) Top Figure: Single diffractive contribution to the classical two particle correlation. Two gluons are emitted from the same quark line in the amplitude and likewise in the complex conjugate amplitude. This diffractive emission however occurs at different spatial positions for the sources, which are localized in a transverse area of size  $1/Q_s$ . See text. There is an identical contribution with  $\rho_1 \leftrightarrow \rho_2$ . b) Bottom Figure: Interference contribution where the transverse positions of the interacting quarks are switched in the complex conjugate amplitude for  $\rho_2$  while they are the same for  $\rho_1$ . There is an identical contribution for  $\rho_1 \leftrightarrow \rho_2$ .

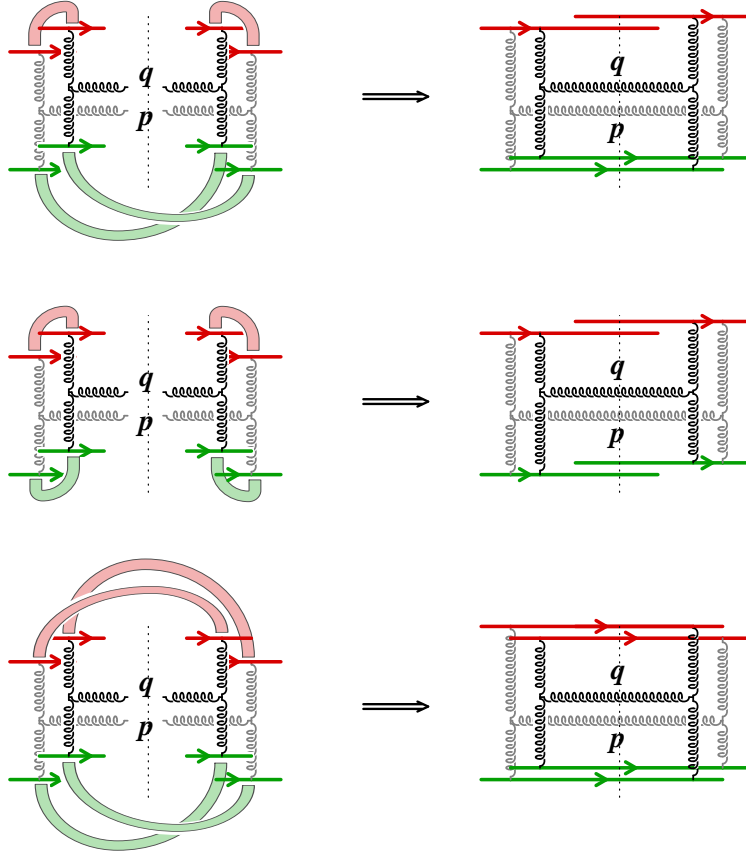


Figure 8: Topology of color correlations. These contributions are detailed in Appendix B. The upper (lower) contractions are pairwise contractions of  $\rho_1$  ( $\rho_2$ ). a) Top Figure: This graph is similar to the single diffractive contribution in fig. 7 (a), except, the emission of the particle with momentum  $p$  in  $\rho_2$  is from different quarks in the amplitude and the complex conjugate amplitude. Likewise for the particle with momentum  $q$ , where the order of quark lines is reversed. There is a similar contribution for  $\rho_1 \leftrightarrow \rho_2$ . b) Middle Figure: Double diffractive contribution. Two gluons are exchanged from a single quark line in both  $\rho_1$  and  $\rho_2$ . As previously for the single diffractive contributions, the quark lines are at different transverse positions in the amplitude and the complex conjugate amplitude. c) Bottom Figure: Non diffractive contribution where all the quarks are swapped in the complex conjugate amplitude.

In our language, the corresponding quantity in the Glasma can be expressed simply as

$$\frac{\Delta\rho}{\sqrt{\rho_{\text{ref}}}} \equiv C(\mathbf{p}, \mathbf{q}) \frac{\langle \frac{dN}{dy} \rangle}{\langle \frac{dN}{dy_p p dp d\phi_p} \rangle \langle \frac{dN}{dy_q q dq d\phi_q} \rangle} = \frac{K_N}{\alpha_s(Q_s)}, \quad (20)$$

where  $\langle dN/dy \rangle$  was defined in eq. (4) and  $K_N = \kappa \kappa' \approx 4/13.5 \sim 0.3$ . Note however that our computation was performed for large  $p_\perp, q_\perp \gg Q_s$  while we are interested in the  $p_\perp, q_\perp \leq Q_s$  region. While we expect the structure of eq. (20) to be quite general, as mentioned earlier, we cannot trust the accuracy of this prefactor. We will therefore only assume it is a number of order unity to be determined by a more accurate numerical computation.

The expression in eq. (20) is very interesting because it is independent both of the rapidities<sup>10</sup>  $y_p$  and  $y_q$  of the particle pairs as well as of their azimuthal angles  $\phi_p$  and  $\phi_q$  respectively. It confirms our picture of flux tubes of transverse size  $1/Q_s$  stretching between the two nuclei (as shown in fig. 4) emitting particles isotropically, with equal probability, along their length. This is not the full picture though. In the high parton density environment created in central heavy ion collisions, the pressure created by interactions among those particles leads to collective radial flow. The particles emitted by the Glasma tubes will also experience this collective flow. As we shall now discuss, this collimates the relative azimuthal distribution of the pairs.

We begin by introducing the rapidities of the particles in the direction of radial flow (the particles azimuthal angles  $\phi_{p,q}$  are defined with respect to the radius of the point of emission),  $\zeta_{p,q} \equiv -\ln(\tan(\phi_{p,q}/2))$ . (It is important to note that the two particles will experience the same radial boost only because they are localized within  $1/Q_s$  of each other in the transverse plane—and therefore lie within the same fluid cell.) Expressing the angular distribution (which is independent of  $\phi_p$  and  $\phi_q$ ) in terms of these variables, and boosting it in the direction of radial flow, one obtains<sup>11</sup>

$$C(\mathbf{p}, \mathbf{q}) \propto \frac{1}{\cosh(\zeta_p) \cosh(\zeta_q)} \xrightarrow{\text{Boost}} \frac{1}{\cosh(\zeta_p - \zeta_B) \cosh(\zeta_q - \zeta_B)}. \quad (21)$$

Here,  $\zeta_B$  is the rapidity of the boost and is given by  $\tanh \zeta_B = V_r$ , where  $V_r$  is the radial flow velocity. Defining  $\Phi = (\phi_p + \phi_q)/2$  and  $\Delta\phi = \phi_p - \phi_q$ , and re-expressing the boosted distribution in terms of  $\Phi$  and  $\Delta\phi$ , one can re-write eq. (20) as

$$\frac{\Delta\rho}{\sqrt{\rho_{\text{ref}}}}(\Phi, \Delta\phi, y_p, y_q) = \frac{K_N}{\alpha_s(Q_s)} \frac{\cosh \zeta_p \cosh \zeta_q}{\cosh(\zeta_p - \zeta_B) \cosh(\zeta_q - \zeta_B)}. \quad (22)$$

<sup>10</sup>Quantum corrections, not considered here, will introduce a modest dependence on rapidity over scales  $\Delta y \sim \alpha_s^{-1}$ .

<sup>11</sup>The hyperbolic cosines in the denominator come from the Jacobian of the change of variables.

Substituting  $\cosh \zeta_p = 1/\sin \phi_p$  and  $\sinh \zeta_p = \cos \phi_p / \sin \phi_p$ , we finally obtain

$$\begin{aligned}
& \int d\Phi \frac{\Delta\rho}{\sqrt{\rho_{\text{ref}}}}(\Phi, \Delta\phi, y_p, y_q) = \\
&= \frac{K_N}{\alpha_s(Q_s)} \int_{-\pi}^{\pi} \frac{d\Phi}{\left[ \cosh \zeta_B - \cos\left(\Phi + \frac{\Delta\phi}{2}\right) \sinh \zeta_B \right] \left[ \cosh \zeta_B - \cos\left(\Phi - \frac{\Delta\phi}{2}\right) \sinh \zeta_B \right]} \\
&= \frac{K_N}{\alpha_s(Q_s)} \frac{2\pi \cosh \zeta_B}{\cosh^2 \zeta_B - \sinh^2 \zeta_B \cos^2 \frac{\Delta\phi}{2}}. \tag{23}
\end{aligned}$$

In the particular cases of  $\Delta\phi = 0$  or  $\Delta\phi = \pi$ , the result is

$$\begin{aligned}
\int d\Phi \frac{\Delta\rho}{\sqrt{\rho_{\text{ref}}}}(\Delta\phi = 0) &= \frac{K_N}{\alpha_s(Q_s)} 2\pi \gamma_B \\
\int d\Phi \frac{\Delta\rho}{\sqrt{\rho_{\text{ref}}}}(\Delta\phi = \pi) &= \frac{K_N}{\alpha_s(Q_s)} \frac{2\pi}{\gamma_B}, \tag{24}
\end{aligned}$$

where  $\gamma_B \equiv \cosh \zeta_B$  is the  $\gamma$ -factor of the boost. Hence, the amplitude of the peak, relative to the pedestal, is given by

$$\mathcal{A} = K_R \frac{\gamma_B - \gamma_B^{-1}}{\alpha_s(Q_s)}. \tag{25}$$

The factor  $K_R$  equals  $2\pi K_N$  times the fraction of detected mini-jets<sup>12</sup>.

From blast wave fits to the RHIC data, the PHENIX collaboration [44] has extracted the average transverse velocity  $\langle V_r \rangle$  as a function of the number of participants in a heavy ion collision. To estimate the centrality dependence of the coupling<sup>13</sup>,  $\alpha_s(Q_s)$ , we note that the square of the saturation momentum  $Q_s^2 \simeq 1\text{-}1.3 \text{ GeV}^2$  for central Au+Au collisions at full RHIC energy, decreasing like  $N_{\text{part}}^{1/3}$  [49] towards peripheral collisions<sup>14</sup>. The magnitude of  $\mathcal{A}$  fixes  $K_R \approx 0.6$ , or  $K_N \sim 0.1$ , in the ballpark of our simple earlier estimate<sup>15</sup>. The resulting  $\mathcal{A}(N_{\text{part}})$  is compared to preliminary STAR data in fig. 9.

The angular width of the correlation function is not reproduced very well by the simple ‘‘radial boost’’ model; the integral from eq. (23), without any prefactors, is shown as a function of  $\Delta\phi$  in fig. 10. The width narrows to  $\simeq 1$  radians only for boost rapidities  $\zeta_B \simeq 2$ , corresponding to boost velocities of about 0.96. To improve the agreement with the measured angular distributions one should probably account also for absorption of high- $p_{\perp}$  particles by the medium [28].

<sup>12</sup>Mini-jets from the center of the nuclei which experience little transverse flow or mini-jets emitted close to the surface are not detected in the ridge. An accurate estimate of the detected mini-jets relative to the total number requires detailed models of the nuclear geometry and flow profiles.

<sup>13</sup>We determine the running coupling from the one-loop QCD  $\beta$ -function with  $\beta_0 = 11N_C - 2N_f = 27$ , assuming  $\Lambda_{\text{QCD}} \simeq 200 \text{ MeV}$ .

<sup>14</sup>The dependence of  $Q_s^2$  on centrality is in fact more complex (we refer to refs. [50]) but the simplified form  $Q_s^2 \sim N_{\text{part}}^{1/3}$  is sufficient for our present purposes.

<sup>15</sup>Note, as previously mentioned that only a fraction of the jets are detected, so this number is closer to our result than one would naively anticipate.



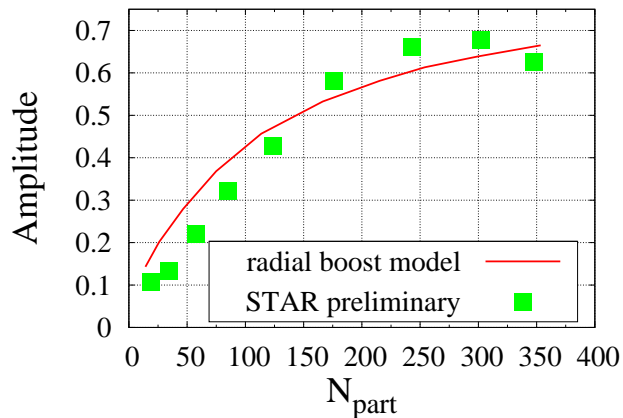


Figure 9: Evolution of the amplitude of the “ridge” (peak at  $\Delta\phi = 0$  relative to pedestal at  $\Delta\phi = \pi$ ) with the number of participants. The preliminary STAR data shown is from ref. [43].

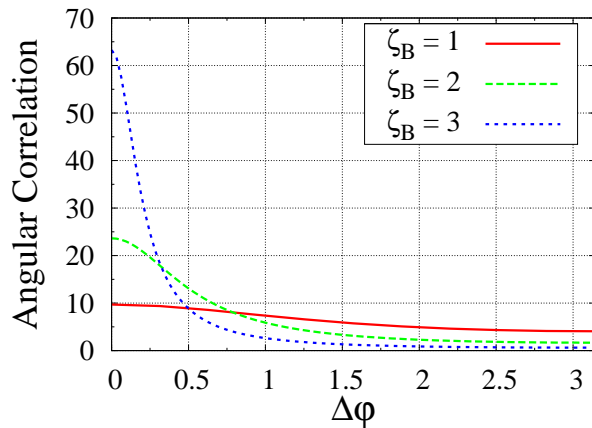


Figure 10: Angular correlation function for three different radial boost rapidities  $\zeta_B$ .

### 3 Discussion

In the previous section we outlined a novel classical contribution to long range rapidity correlations in the Glasma. Boost invariant Glasma flux tubes of size  $1/Q_s$  in the transverse plane of the nuclei produce particles isotropically with equal probability along the length of the flux tube. The common transverse expansion experienced by particles in a flux tube collimates the particles forming a ridge like structure in the process. Our result provides a qualitative explanation of several features of the ridge [23,24,43,35] in addition to those we discussed above. We outline these below.

- The classical two gluon contribution identified here is qualitatively different from the usual jet mechanism of two particle correlations. It has the same structure as single gluon production. This strongly suggests that the particles forming the ridge have the same particle composition as the bulk spectra.
- The large classical two gluon contribution qualitatively explains the large multiplicity of particles in the ridge relative to particles in the bulk; indeed, we obtain a ratio of order unity naively but this needs to be corrected for the fraction of “mini-jets” that are not detected. Estimating this accurately requires detailed modeling. However, naively comparing our model computation to the experimental result, we can guess that this factor is about a third of all mini-jets. This contribution increases with centrality and energy because  $Q_s$  is a function of both.
- The ridge appears independent of the trigger  $p_\perp$  and is seen for associated particles both with a minimal  $p_\perp$  cut and for  $p_{\perp,\text{assoc.}} \geq 2$  GeV. Our result was derived at large  $p_\perp$ , but has a geometrical form that seems very general and plausible for low  $p_\perp$  particles as well. The form of our high  $p_\perp$ ,  $q_\perp$  result suggests that the ridge yield is insensitive to the trigger  $p_\perp$ . At high  $p_\perp$ , it is unlikely the collimation in azimuthal angle is provided by transverse flow; it may instead be an opacity effect resulting from the strong dependence of the energy loss of partons on the path length traversed in the medium.
- The ridge amplitude in our model is determined by  $Q_s^2$  and the average transverse velocity  $\langle V_r \rangle$ . Both of these quantities grow with the centrality (number of participants) and the collision energy. As the transverse particle density also grows with centrality and collision energy, it is plausible that one obtains an approximate scaling of the ridge amplitude as a function of the transverse particle density rather than with the energy and centrality separately.
- A study of unlike and like sign charge pairs by STAR [48] shows that for small  $\Delta\eta$ , the signal for unlike sign charge pairs dominates over that for like sign pairs, as one would anticipate from jet fragmentation. However, for large  $\Delta\eta$ , the signal for like and unlike sign pairs is the same. This

is consistent with a picture of correlated charge neutral sources, such as gluons in our case, widely separated in rapidity, emitting opposite charge pairs. With such emissions, like sign pairs and unlike sign pairs are equally likely to be correlated, just as seen in the data.

A more quantitative comparison to the ridge data requires more detailed numerical computations. Nevertheless, it is encouraging that qualitative features of the ridge are consistent with the formation and flow of Glasma flux tubes. We should also note that our picture has features in common with those deduced [47] from an analysis of the azimuthal correlation data at RHIC.

## Acknowledgments

This work was initiated under the project ‘‘Yukawa International Program for Quark-Hadron Sciences’’ at the Yukawa Institute for Theoretical Physics of the University of Kyoto. We thank the organizers for the stimulating atmosphere and for their kind hospitality. We would also like to thank Jean-Paul Blaizot, Michael Daugherty, Jamie Dunlop, Tuomas Lappi, Ron Longacre, Paul Sorensen and Nu Xu for very valuable discussions. LM and RV’s research is supported by DOE Contract No. DE-AC02-98CH10886. F.G.’s work is supported in part by Agence Nationale de la Recherche via the programme ANR-06-BLAN-0285-01.

## Appendix A

We shall first compute the ‘‘single diffractive’’ diagram in fig. 7(a). Performing the contractions among the  $\rho$ ’s corresponding to this graph, we can write this contribution to eq. (12) as

$$\begin{aligned} \mathcal{F}^{(1)} &= (2\pi)^8 \mu_A^8 \delta^{\hat{b}b} \delta^{\hat{b}\bar{b}} \delta^{\hat{c}\bar{c}} \delta^{c\bar{c}} \delta(\mathbf{k}_{1\perp} - \mathbf{k}_{2\perp}) \delta(\mathbf{k}_{3\perp} - \mathbf{k}_{4\perp}) \\ &\quad \times \delta(\mathbf{q}_\perp + \mathbf{p}_\perp - \mathbf{k}_{3\perp} - \mathbf{k}_{1\perp}) \delta(\mathbf{q}_\perp + \mathbf{p}_\perp - \mathbf{k}_{4\perp} - \mathbf{k}_{2\perp}), \end{aligned} \quad (26)$$

where the superscript denotes the contribution of this particular graph. Substituting this expression in eq. (10), we obtain correspondingly,

$$C^{(1)}(\mathbf{p}, \mathbf{q}) = \frac{N_c^2(N_c^2 - 1)}{64(2\pi)^6} \frac{(g^2 \mu_A)^8}{g^4} S_\perp \int d^2 \mathbf{k}_{1\perp} \mathcal{A}^{(1)}(\mathbf{p}_\perp, \mathbf{k}_{1\perp}) \mathcal{A}^{(1)}(\mathbf{q}_\perp, -\mathbf{k}_{1\perp}), \quad (27)$$

where  $S_\perp$  is the transverse overlap area of the nuclei and<sup>16</sup> where

$$\mathcal{A}^{(1)}(\mathbf{p}_\perp, \mathbf{k}_{1\perp}) = -\frac{4}{p_\perp^2} \frac{[(\mathbf{p}_\perp + \mathbf{k}_{1\perp}) \cdot \mathbf{k}_{1\perp}]^2 + [\mathbf{p}_\perp \times \mathbf{k}_{1\perp}]^2}{k_{1\perp}^4 (\mathbf{p}_\perp + \mathbf{k}_{1\perp})^4}. \quad (29)$$

Studying the structure of eq. (29), it is clear that the terms with the fewest powers of  $\mathbf{p}_\perp, \mathbf{q}_\perp$  in the denominator (and therefore the largest contribution to  $C_1^{(1)}$ ) are those with the fewest powers of  $\mathbf{k}_{1\perp}$  in the numerator. One then finds simply that

$$\mathcal{A}^{(1)}(\mathbf{p}_\perp, \mathbf{k}_{1\perp}) \mathcal{A}^{(1)}(\mathbf{q}_\perp, -\mathbf{k}_{1\perp}) \longrightarrow \frac{16}{p_\perp^4 q_\perp^4} \frac{1}{k_{1\perp}^4}. \quad (30)$$

Note that the angular dependence on the relative angles of  $\mathbf{k}_{1\perp}$  with  $\mathbf{p}_\perp$  and  $\mathbf{q}_\perp$  cancels between the leading longitudinal and transverse contributions to eq. (29). Substituting this result back into eq. (27), this gives

$$C^{(1)}(\mathbf{p}, \mathbf{q}) = \frac{S_\perp}{4(2\pi)^6} \frac{(g^2 \mu_A)^8}{g^4 Q_s^2} \frac{\pi N_c^2 (N_c^2 - 1)}{p_\perp^4 q_\perp^4}, \quad (31)$$

where we have used the infrared cut-off  $k_{\min} = Q_s$ , which is the saturation scale signifying the onset of non-linear contributions that soften the infrared gluon distributions in the CGC.

We now turn to the ‘‘interference diagram’’ diagram in fig. 7(b). Again, performing the contractions among the  $\rho$ 's corresponding to this graph, we can write this contribution to eq. (12) as

$$\begin{aligned} \mathcal{F}^{(2)} &= (2\pi)^8 \mu_A^8 \delta^{\hat{b}\hat{b}} \delta^{\hat{b}\hat{b}} \delta^{\hat{c}\hat{c}} \delta^{\hat{c}\hat{c}} \delta(\mathbf{k}_{1\perp} - \mathbf{k}_{2\perp}) \delta(\mathbf{k}_{3\perp} - \mathbf{k}_{4\perp}) \\ &\quad \times \delta(\mathbf{p}_\perp - \mathbf{q}_\perp - \mathbf{k}_{3\perp} + \mathbf{k}_{2\perp}) \delta(\mathbf{q}_\perp - \mathbf{p}_\perp + \mathbf{k}_{1\perp} - \mathbf{k}_{4\perp}), \end{aligned} \quad (32)$$

where the superscript denotes the contribution of this particular graph. Again, plugging this in eq. (10), we obtain,

$$C^{(2)}(\mathbf{p}, \mathbf{q}) = \frac{N_c^2 (N_c^2 - 1)}{64 (2\pi)^6} \frac{(g^2 \mu_A)^8}{g^4} S_\perp \int d^2 \mathbf{k}_{1\perp} \mathcal{A}^{(1)}(\mathbf{p}_\perp, \mathbf{k}_{1\perp}) \mathcal{A}^{(1)}(\mathbf{q}, \mathbf{k}_{1\perp}). \quad (33)$$

The leading contribution to the integrand is the same as in eq. (30), and we obtain

$$C^{(2)}(\mathbf{p}, \mathbf{q}) = \frac{S_\perp}{4(2\pi)^6} \frac{(g^2 \mu_A)^8}{g^4 Q_s^2} \frac{\pi N_c^2 (N_c^2 - 1)}{p_\perp^4 q_\perp^4}, \quad (34)$$

which is identical to eq. (31).

---

<sup>16</sup>In general,

$$\mathcal{A}(\mathbf{p}_\perp, \mathbf{k}_{1\perp}, \mathbf{k}_{2\perp}) = \frac{L_\mu(\mathbf{p}, \mathbf{k}_{1\perp}) L^\mu(\mathbf{p}, \mathbf{k}_{2\perp})}{\mathbf{k}_{1\perp}^2 (\mathbf{p}_\perp - \mathbf{k}_{1\perp})^2 \mathbf{k}_{2\perp}^2 (\mathbf{p}_\perp - \mathbf{k}_{2\perp})^2}, \quad (28)$$

where the product of Lipatov vertices is given in eq. (11). In eq. (27), we use the notation  $\mathcal{A}(\mathbf{p}_\perp, \mathbf{k}_{1\perp}, \mathbf{k}_{1\perp}) \equiv \mathcal{A}^{(1)}(\mathbf{p}_\perp, \mathbf{k}_{1\perp})$ .

The other two leading “single diffractive” and “interference” contributions, which we label by  $C^{(3)}$  and  $C^{(6)}$  respectively, have a structure such that

$$\begin{aligned} C^{(3)} &\longleftrightarrow C^{(1)} \text{ for } \rho_1 \longleftrightarrow \rho_2 \\ C^{(6)} &\longleftrightarrow C^{(2)} \text{ for } \rho_1 \longleftrightarrow \rho_2, \end{aligned} \quad (35)$$

so it is not surprising that these terms give contributions that are identical to eqs. (31) and (34).

## Appendix B

We now turn to the topologies discussed in fig. 8. Consider first the topology shown in fig. 8(a). We obtain in this case the contribution to eq. (12) as

$$\begin{aligned} \mathcal{F}^{(5)} &= (2\pi)^8 \mu_A^8 \delta^{\hat{b}\bar{b}} \delta^{b\bar{b}} \delta^{\hat{c}\bar{c}} \delta^{c\bar{c}} \delta(\mathbf{k}_{1\perp} + \mathbf{k}_{3\perp}) \delta(\mathbf{k}_{2\perp} + \mathbf{k}_{4\perp}) \\ &\quad \times \delta(\mathbf{p}_\perp - \mathbf{q}_\perp - \mathbf{k}_{2\perp} + \mathbf{k}_{3\perp}) \delta(\mathbf{q}_\perp - \mathbf{p}_\perp - \mathbf{k}_{4\perp} + \mathbf{k}_{1\perp}), \end{aligned} \quad (36)$$

where the superscript denotes the contribution of this graph. Again, substituting this expression in eq. (10), we obtain

$$\begin{aligned} C^{(5)}(\mathbf{p}, \mathbf{q}) &= \frac{1}{64(2\pi)^6} \frac{N_c^2(N_c^2 - 1)}{2} \frac{(g^2 \mu_A)^8}{g^4} S_\perp \\ &\quad \times \int d^2 \mathbf{k}_\perp \mathcal{A}(\mathbf{p}_\perp, \mathbf{k}_\perp, \mathbf{p}_\perp - \mathbf{q}_\perp - \mathbf{k}_\perp) \mathcal{A}(\mathbf{q}_\perp, -\mathbf{k}_\perp, \mathbf{q} - \mathbf{p} + \mathbf{k}_\perp), \end{aligned} \quad (37)$$

where, from eq. (28),

$$\begin{aligned} \mathcal{A}(\mathbf{p}_\perp, \mathbf{k}_\perp, \mathbf{p}_\perp - \mathbf{q}_\perp - \mathbf{k}_\perp) &= -\frac{4}{p_\perp^2} \\ &\quad \times \frac{\left[ (\mathbf{p}_\perp - \mathbf{k}_\perp) \cdot \mathbf{k}_\perp (\mathbf{p}_\perp - \mathbf{q}_\perp - \mathbf{k}_\perp) \cdot (\mathbf{q}_\perp + \mathbf{k}_\perp) \right. \\ &\quad \left. + (\mathbf{k}_\perp \times (\mathbf{p}_\perp - \mathbf{k}_\perp)) \cdot ((\mathbf{p}_\perp - \mathbf{q}_\perp - \mathbf{k}_\perp) \times (\mathbf{q}_\perp + \mathbf{k}_\perp)) \right]}{k_\perp^2 (\mathbf{p}_\perp - \mathbf{k}_\perp)^2 (\mathbf{p}_\perp - \mathbf{q}_\perp - \mathbf{k}_\perp)^2 (\mathbf{q}_\perp + \mathbf{k}_\perp)^2}, \end{aligned} \quad (38)$$

and likewise, a similar expression for  $\mathcal{A}(\mathbf{q}_\perp, -\mathbf{k}_\perp, \mathbf{q}_\perp - \mathbf{p}_\perp + \mathbf{k}_\perp)$ . Unlike the expression in eq. (30), this expression does not have a simple expression in the infrared. It is however suppressed by additional powers of  $\mathbf{p}_\perp$  and  $\mathbf{q}_\perp$  relative to the leading terms, allowing us to ignore this sub-dominant contribution. There is another contribution, that we denote by  $C^{(7)}$ , obtained by exchanging  $\rho_1 \leftrightarrow \rho_2$  in fig. 8 (a) that is similarly suppressed.

Finally, there are the diagrams discussed in fig. 8 (b) and (c). The former has the form of a “double diffractive” contribution. We denote its contribution to eq. (12) by

$$\begin{aligned} \mathcal{F}^{(4)} &= (2\pi)^8 \mu_A^8 \delta^{\hat{b}\bar{b}} \delta^{b\bar{b}} \delta^{\hat{c}\bar{c}} \delta^{c\bar{c}} \delta(\mathbf{k}_{1\perp} + \mathbf{k}_{3\perp}) \delta(\mathbf{k}_{2\perp} + \mathbf{k}_{4\perp}) \\ &\quad \times \delta(\mathbf{p}_\perp + \mathbf{q}_\perp - \mathbf{k}_{2\perp} - \mathbf{k}_{4\perp}) \delta(\mathbf{q}_\perp + \mathbf{p}_\perp - \mathbf{k}_{1\perp} - \mathbf{k}_{3\perp}). \end{aligned} \quad (39)$$

From the structure of this equation, we will have

$$C^{(4)}(\mathbf{p}, \mathbf{q}) = \frac{N_c^2(N_c^2 - 1)}{64(2\pi)^6} \frac{(g^2\mu_A)^8}{g^4} S_\perp \delta(\mathbf{p}_\perp + \mathbf{q}_\perp) \\ \times \int d^2\mathbf{k}_{1\perp} d^2\mathbf{k}_{2\perp} \mathcal{A}(\mathbf{p}_\perp, \mathbf{k}_{1\perp}, \mathbf{k}_{2\perp}) \mathcal{A}(-\mathbf{p}_\perp, -\mathbf{k}_{1\perp}, -\mathbf{k}_{2\perp}), \quad (40)$$

where the form of  $\mathcal{A}$  is obtained from eq. (28). One obtains a similar expression for fig. 8(c), where instead of a  $\delta$ -function in  $\mathbf{p}_\perp + \mathbf{q}_\perp$ , one gets instead a  $\delta$ -function in  $\mathbf{p}_\perp - \mathbf{q}_\perp$ . These  $\delta$ -functions will be smeared out by re-scattering and are suppressed relative to the leading terms in Appendix A.

## References

- [1] L.D. McLerran, R. Venugopalan, Phys. Rev. **D 49**, 2233 (1994). *ibid.* **D 49**, 3352 (1994); **D 50**, 2225 (1994).
- [2] Yu.V. Kovchegov, Phys. Rev. **D 54**, 5463 (1996).
- [3] E. Iancu, R. Venugopalan, Quark Gluon Plasma 3, Eds. R.C. Hwa, X.N.Wang, World Scientific, hep-ph/0303204.
- [4] A. Kovner, L.D. McLerran, H. Weigert, Phys. Rev. **D 52**, 3809 (1995); *ibid.*, **D 52**, 6231 (1995).
- [5] A. Krasnitz, R. Venugopalan, Nucl. Phys. **B 557**, 237 (1999); Phys. Rev. Lett. **84**, 4309 (2000); Phys. Rev. Lett. **86**, 1717 (2001).
- [6] A. Krasnitz, Y. Nara, R. Venugopalan, Phys. Rev. Lett. **87**, 192302 (2001); Nucl. Phys. **A 727**, 427 (2003).
- [7] T. Lappi, Phys. Rev. **C 67**, 054903 (2003).
- [8] T. Lappi, L. McLerran, Nucl. Phys. **A 772**, 200 (2006).
- [9] F. Gelis, R. Venugopalan, Acta Phys. Polon. B **37**, 3253 (2006).
- [10] F. Gelis, R. Venugopalan, Nucl. Phys. **A 776**, 135 (2006); *ibid.*, **A 779**, 177 (2006); F. Gelis, T. Lappi, R. Venugopalan, Int. J. Mod. Phys. E **16**, 2595 (2007); arXiv:0804.2630 [hep-ph].
- [11] Yu.V. Kovchegov, D.H. Rischke, Phys. Rev. **C 56**, 1084 (1997).
- [12] R. J. Fries, J. Phys. G **34**, S851 (2007).
- [13] D. Kharzeev, A. Krasnitz, R. Venugopalan, Phys. Lett. **B 545**, 298 (2002).
- [14] Y. Kovchegov E. Levin, L. McLerran, Phys. Rev. **C63**:024903 (2001).
- [15] S. Uhlig, I. Derado, R. Meinke and H. Preissner, Nucl. Phys. B **132**, 15 (1978).

- [16] B. Andersson, G. Gustafson, G. Ingelman, T. Sjostrand, Phys. Rept. **97**, 31 (1983).
- [17] A. Capella, U. Sukhatme, C. I. Tan, J. Tran Thanh Van, Phys. Rept. **236**, 225 (1994); A. Capella, A. Krzywicki, Phys. Rev. D **18**, 4120 (1978).
- [18] N. S. Manton, Phys. Rev. **D28** 2019 (1983); F. Klinkhammer, N. Manton, Phys. Rev. **D30** 2212 (1984).
- [19] V. Kuzmin, V. Rubakov, M. Shaposhnikov, Phys. Lett. **B155** (1985).
- [20] M. Diakonov, Y. Petrov, Nucl. Phys. **B272** 457 (1986).
- [21] Brijesh Srivastava for the STAR Collaboration, Int. J. Mod. Phys. **E16**, 3371 (2008).
- [22] N. Armesto, L. McLerran, C. Pajares, Nucl. Phys. A **781**, 201 (2007).
- [23] J. Adams et al. [STAR Collaboration] Phys. Rev. Lett. **95**:152301, (2005); Fuqiang Wang [STAR Collaboration], talk at Quark Matter 2004, J. Phys. G **30**:S1299-S1304, (2004).
- [24] J. Adams *et al.* [STAR Collaboration], Phys. Rev. C **73**, 064907 (2006).
- [25] A. Adare *et al.* [PHENIX Collaboration], arXiv:0801.4545 [nucl-ex].
- [26] B. Wosiek, [PHOBOS Collaboration], Plenary Talk at Quark Matter 2008, Jaipur, India, Feb. 4th-10th, 2008.
- [27] S. A. Voloshin, Phys. Lett. B **632**, 490 (2006).
- [28] E. V. Shuryak, Phys. Rev. C **76**, 047901 (2007).
- [29] C. A. Pruneau, S. Gavin, S. A. Voloshin, Nucl. Phys. A **802**, 107 (2008).
- [30] N. Armesto, C. A. Salgado, U. A. Wiedemann, Phys. Rev. Lett. **93**, 242301 (2004); P. Romatschke, Phys. Rev. C **75**, 014901 (2007); A. Majumder, B. Muller, S. A. Bass, Phys. Rev. Lett. **99**, 042301 (2007); C. B. Chiu, R. C. Hwa, Phys. Rev. C **72**, 034903 (2005); C. Y. Wong, arXiv:0712.3282 [hep-ph]; R. C. Hwa, C. B. Yang, arXiv:0801.2183 [nucl-th]; T. A. Trainor, arXiv:0708.0792 [hep-ph]; A. Dumitru, Y. Nara, B. Schenke, M. Strickland, arXiv:0710.1223 [hep-ph].
- [31] E. Komatsu *et al.* [WMAP Collaboration], arXiv:0803.0547 [astro-ph].
- [32] H. Kowalski, T. Lappi, R. Venugopalan, Phys. Rev. Lett. **100**, 022303 (2008).
- [33] B. K. Srivastava [STAR Collaboration], Int. J. Mod. Phys. E **16**, 3371 (2008); B. K. Srivastava, R. P. Scharenberg, T. J. Tarnowsky, arXiv:nucl-ex/0702040.

- [34] F. Gelis, T. Lappi, R. Venugopalan, work in preparation.
- [35] J. Putschke [STAR Collaboration], J. Phys. G **34**, S679 (2007);
- [36] A. Dumitru, L. D. McLerran, Nucl. Phys. **A 700**, 492 (2002).
- [37] J.P. Blaizot, F. Gelis, R. Venugopalan, Nucl. Phys. **A 743**, 13 (2004).
- [38] I. I. Balitsky and L. N. Lipatov, Sov. J. Nucl. Phys. **28**, 822 (1978).
- [39] I. Balitsky, Nucl. Phys. **B 463**, 99 (1996); Yu.V. Kovchegov, Phys. Rev. **D 61**, 074018 (2000).
- [40] Y. V. Kovchegov, L. D. McLerran, Phys. Rev. D **60**, 054025 (1999) [Erratum-ibid. D **62**, 019901 (2000)].
- [41] J. F. Gunion, G. Bertsch, Phys. Rev. D **25**, 746 (1982).
- [42] M. Gyulassy, L. D. McLerran, Phys. Rev. C **56**, 2219 (1997).
- [43] M. Daugherty [STAR Collaboration], talk at Quark Matter 2008, Jaipur, India, Feb. 4th-10th, 2008, to be published in conference proceedings.
- [44] A. Kiyomichi [PHENIX Collaboration], *Prepared for Lake Louise Winter Institute: Fundamental Interactions, Lake Louise, Alberta, Canada, 20-26 Feb 2005.*
- [45] T. Lappi, arXiv:0711.3039 [hep-ph].
- [46] K. Fukushima, arXiv:0711.2364 [hep-ph].
- [47] S. J. Lindenbaum, R. S. Longacre, Eur. Phys. J. C **49**, 767 (2007).
- [48] J. Adams et al., [STAR Collaboration], Phys. Rev. C **75**, 034901 (2007).
- [49] D. Kharzeev and M. Nardi, Phys. Lett. B **507**, 121 (2001); D. Kharzeev and E. Levin, Phys. Lett. B **523**, 79 (2001).
- [50] H. J. Drescher *et al.*, Phys. Rev. C **74**, 044905 (2006) [arXiv:nucl-th/0605012]; Phys. Rev. C **75**, 034905 (2007) [arXiv:nucl-th/0611017]; T. Lappi and R. Venugopalan, Phys. Rev. C **74**, 054905 (2006) [arXiv:nucl-th/0609021].